J. Space Weather Space Clim. 2025, **15**, 14

https://doi.org/10.1051/swsc/2025007

JSWSC

Available online at:
www.swsc-journal.org

RESEARCH ARTICLE OPEN ACCESS

Solar flare rates and probabilities based on the McIntosh classification: Impacts of GOES/XRS rescaling and revisited sunspot classifications

Jan Janssens[1,*], Véronique Delouille[2], Frédéric Clette[2,3], and Jesse Andries[2]

[1] Solar-Terrestrial Centre of Excellence (STCE), Royal Observatory of Belgium, Avenue Circulaire 3, 1180 Brussels, Belgium
[2] Royal Observatory of Belgium, Avenue Circulaire 3, 1180 Brussels, Belgium
[3] Institut d'Astronomie et d'Astrophysique, Brussels Laboratory of the Universe (BLU), Université Libre de Bruxelles, CP 226, Avenue F. Roosevelt 50, 1050 Brussels, Belgium

Received 12 July 2024 / Accepted 25 February 2025

Abstract – In December 2019, the Space Weather Prediction Center (SWPC) started using the GOES[1]-16 satellite as its primary input for solar X-ray flux monitoring. As such, it stopped applying a scaling factor that had been applied since the GOES-8 came into operation. This has an important impact on the number of flares that can be expected and on the flare rates associated with the McIntosh classifications, which are often used to help forecast flare activity. To quantify the effects, the flare intensities for the period covering 1976–2019 have all been recalculated. An increase of respectively 55% and 52% in the total number of M-class and X-class events has been observed. Also, for the same period, McIntosh classifications have been redone by visually evaluating 4720 Kanzelhöhe solar drawings (about 1 drawing every 3 days) and determining the McIntosh type of 22232 sunspot regions. There is an excellent agreement with the values originally reported by McIntosh (1990), but some deviations from the SWPC data are found. For a majority of the McIntosh classes, an increase in the flare rates is observed, which translates into increased flare probabilities assuming a Poisson distribution for the flare occurrence. This is an important given for space weather forecasters when making solar flare forecasts. The McIntosh classification is successful in distinguishing flare active from flare inactive regions: Considering only the "p" and "c" components of the McIntosh classification and linking them to the number of flares associated with the corresponding sunspot groups, we find that 48% of all M- and X-class flares in our study are produced by only 8% of all sunspot groups, belonging to the McIntosh subclasses -ai, -kc, and -ki corresponding to sunspot groups with an asymmetric main spot and a more complex (intermediate or compact) internal sunspot distribution. About 57% of all classified sunspot groups produce only 12% of all M- and X-class flares. They belong to the McIntosh subclasses -so, -sx, -xo, and -xx, which correspond to the smallest and simplest sunspot regions and the phases marking the emergence and final decay of sunspot groups (Axx, Bxo, Hsx). Though the McIntosh classification is a great tool to forecast flare activity, there remain large differences in the actual flare behaviour of individual sunspot groups within the same McIntosh class.

Keywords: McIntosh classification / Solar flares / Flare probability / GOES / Sunspot group

1 Introduction

Solar flares belong to the most energetic events in the solar system. The X-ray and extreme ultraviolet (EUV) emission released by these explosive events disturbs the Earth's ionosphere, thus affecting high-frequency communication (HF Com; 3–30 MHz), as described by the NOAA R-scale[2] (Radio blackout; Poppe, 2000). Occasionally, the flare events are also accompanied by strong emission at radio frequencies greater than 30 MHz (Hey, 1946; Boischot, 1958). These "Type IV" radio bursts may significantly deteriorate satellite signals (e.g. Cerruti et al., 2008) as well as ground-based radar

*Corresponding author: jan.janssens@oma.be
[1] GOES: Geostationary Operational Environmental Satellites.

[2] NOAA (National Oceanic and Atmospheric Administration) space weather scales: https://www.swpc.noaa.gov/noaa-scales-explanation.

operations at the affected frequencies (e.g. Marqué et al., 2018). Since the first (white light) detection of a solar flare on 1 September 1859 (Carrington, 1859), experience by space weather forecast centers has proven that it is not such an easy task to forecast the correct timing and intensity of a solar flare (e.g. Devos et al., 2014; Kubo et al., 2017; Murray et al., 2017). This is a nuisance for various space weather (SWx) end users who rely on the proper functioning of these technology-based services and infrastructure.

Recognizing the important space weather effects that solar flares can induce, researchers have developed various forecasting schemes over the years. An overview and discussion of the flare forecasting methods and their performance can be found in Barnes et al. (2016) and Leka et al. (2019a, 2019b). These methodologies allow the forecast of flare probabilities, usually over a period of 24 hours, and for a range of flare intensities designated by the GOES flare class (A, B, C, M, and X – see Sect. 2.1). A widely used scheme is based on the McIntosh sunspot group classification (McIntosh 1990 – henceforth McI90). Here, sunspot groups are binned into 60 categories according to their size, length, shape of the main sunspot's penumbra, and internal sunspot distribution. Then, for each category, the flare frequency is determined for the 3 main GOES X-ray classes C, M, and X, whereas the weaker A- and B-class flares are mostly ignored in the flare forecasts. Applying these numbers to the observed sunspot regions, the SWx forecaster can then determine the solar flare probabilities for any given day.

The accuracy of the flare predictions that are based solely on the McIntosh classification leaves room for improvement (see e.g. Barnes et al., 2016; Park et al., 2020). SWx forecasters fine-tune the numbers by also looking at the magnetic structure of each sunspot group (Mount Wilson classification; Hale et al., 1919; Künzel 1960), which may be combined with the sunspot area (Sammis et al., 2000), the evolution of the sunspot area (Lee et al., 2012), the presence of specific group features such as filaments or sigmoids (Canfield et al., 1999) in the active region, or small scale structures that can act as flare triggers (e.g. Kusano et al., 2020). Extensive discussions on the various physical mechanisms behind solar flares can be found in e.g. Kowalski (2024) and Toriumi & Wang (2019).

Attempts have also been undertaken to simplify the McIntosh classification scheme (Bornmann & Shaw, 1994), to apply a different methodology for relating the categories to the flare statistics (Bornmann et al., 1994), or even to take into account the evolution from one McIntosh category to another (McCloskey et al., 2016, 2018 – henceforth McC16 and McC18 respectively). Several research groups have also developed other methodologies, such as automated McIntosh class assignments to sunspot groups, including the use of machine learning techniques (e.g. Qahwaji & Colak, 2007; Lee et al., 2013, ASSA[3]). Whereas the McIntosh classification is inherently qualitative by nature, other machine-learning techniques based on quantitative photospheric features derived from magnetograms were proposed (Leka et al., 2019b). But in all methods, the flare probability forecast may still not match the observed flare frequencies, not in the least because of the sometimes unexpected nature of the solar flare production, reminding researchers that there are still unknown processes governing some of the fundamental physics of flare generation.

Since 2000, the Solar Influences Data analysis Center (SIDC) at the Royal Observatory of Belgium (ROB) has a SWx forecast team that provides daily space weather bulletins (the so-called URSIgrams[4]), containing – among others – an analysis of the solar flare activity and a 1-day forecast of the flare probabilities.[5] This forecast is based on McIntosh classifications provided by NOAA, Catania[6], and their own assessment. In doing so, it became clear that the NOAA classifications occasionally tended to the high side, sometimes attributing sunspot groups too compact sunspot distributions and overestimating the size and asymmetry of the main sunspot (see Sect. 3.1). As a result, the flare forecast probabilities solely based on NOAA's McIntosh classifications were too high. NOAA obtains the McIntosh classifications from the Solar Observing Optical Network (SOON[7]; Giersch et al., 2018) maintained by the United States Air Force (USAF). As a result, these McIntosh classifications and other sunspot group data, such as the sunspot area, pertain to sunspot groups from the previous day. Thus, the NOAA data, as imported into the SIDC's flare forecasting system, may sometimes also be somewhat outdated to keep up with some of the fast-evolving, more complex sunspot groups, which results in inaccurate flare probabilities.

In December 2019, with GOES-16 becoming the primary satellite for solar X-ray flux monitoring, NOAA's Space Weather Prediction Center (SWPC) stopped applying a correction factor to the recorded X-ray fluxes[8] ("0.7" for the XRSB Long Channel covering from 0.1 to 0.8 nm). These scaling factors were initially implemented by SWPC to get GOES-8 fluxes to agree with GOES-7, as GOES-7 was the last of the spinning GOES satellites while GOES-8 was the first of the three-axis-stabilized satellites. Since then, rocket launches and comparisons with the new well-calibrated GOES-16 have confirmed that the GOES-8 through GOES-15 sensors are accurate and that the use of scaling factors to match the old spinning satellites is not correct. Therefore, the X-ray fluxes reported by previous GOES satellites (prior to GOES-16) are lower than the currently reported ones (i.e. from GOES-16 and onwards). This basically means that a flare reported by the old reporting system (GOES-15 and earlier) as a C7 flare is, in reality, an M1 flare. Under the new reporting system (from GOES-16 onwards), it would have effectively been reported as an M1

[3] ASSA: Automatic Solar Synoptic Analyzer (Korea Space Weather Center) – https://spaceweather.kasa.go.kr/assa (Hong et al., 2014 – https://ui.adsabs.harvard.edu/abs/2014AGUFMSH21A4089H/abstract).

[4] URSI: Union Radio-Scientifique Internationale – International Union of Radio Science.

[5] Only the flare probability for the next 24 hours is mentioned in the URSIgram. The 24 hours flare probability for day 2 and day 3 are also determined, but are not published and kept for internal use.

[6] The Catania data are available at http://web.ct.astro.it/sun/.

[7] The daily Solar Region Summaries are available at NOAA/SWPC's website: https://www.swpc.noaa.gov/products/solar-region-summary.

[8] A discussion and some background is provided by NOAA/NCEI (National Centers for Environmental Information) and can be found on their website at https://www.ngdc.noaa.gov/stp/satellite/goes/index.html (GOES X-ray Sensor), as well as in this SWPC newsitem at https://www.swpc.noaa.gov/news/goes-14-15-are-now-storage-mode.

flare. The strongest flare in the database, an X28 event observed on 4 November 2003, would now count as an X40 flare. Consequently, a larger number of M- and X-class flares can be expected for the same McIntosh categories than in the pre-GOES-16 era, when the downscaling factor of 0.7 was applied. As such, the flare rates for the various McIntosh classes, as obtained by earlier studies, would considerably underestimate the flare activity for the various McIntosh classifications, especially for the larger and more complex classes.

The contribution of our study is three-fold. First, as described in Section 2, the 0.7 downscaling factor was removed from the old GOES data for the period 1976–2019. The number of flares for each category was recalculated ("GOES new") and compared to the old GOES data ("GOES old"). For the same period, as described in Section 3, the McIntosh sunspot group classifications were redone, and the overall numbers for each category were compared to already published material (McI90; Bloomfield et al., 2012; henceforth BL12). In Section 4, the flare rate for each of the 60 McIntosh categories is computed. These "new" flare rates are compared with "old" values previously published by e.g. BL12, and conclusions with respect to flare prediction using sunspot McIntosh classification are drawn. As far as we know, our study is the first to compile flare rates and flare probabilities based on these rescaled flare intensities and revised McIntosh classifications. Section 5 provides a summary of our main conclusions.

2 GOES flare statistics

2.1 Introduction

GOES, the Geostationary Operational Environmental Satellites, has been providing SWx data since 1976. One of its instruments, the soft X-ray sensor (XRS), monitors the global solar irradiance in two wavelength bands of 0.05 to 0.4 nm (short channel) and 0.1 to 0.8 nm (long channel). The choice for the 0.1–0.8 nm band over other solar indices, such as the 10.7 cm solar radio flux or H-alpha observations, had several reasons, the main being that the X-ray emission from a strong solar flare has important ionization effects in the Earth's ionosphere. Other advantages were that there are no center-to-limb effects, that the source of the flare is confined to the corona, thus avoiding any contribution from e.g. the quiet chromosphere, and that there is an obvious range up to 3 orders of magnitude between solar cycle (SC) minimum and maximum (Bouwer, 1983, Aschwanden 1994). The other, harder X-ray channel (0.05–0.4 nm) provides additional information on the state of the coronal plasma (Garcia, 1994), on spectral hardness (White et al., 2005) and is used in other research such as e.g. on the onset of solar flares (Hudson et al., 2021).

The GOES X-ray sensors take measurements every 3 seconds[9] using two gas-filled ion-chambers (Aschwanden, 1994). They operate on the ion-chamber principle: measured ion-chamber electric current is proportional to the net ionization rate caused by incident X-ray flux on encapsulated noble gases. A description and procedure of the computation are provided by Garcia (1994). Based on the obtained output, Don Baker created the NOAA's flare classification scheme labeled "A-B-C-M-X" (Poppe & Jorden, 2006), which is defined on a logarithmic scale as follows: soft X-ray classes A1-9 through X1-9 correspond to flare peak 0.1–0.8 nm fluxes of $1–9 \times 10^{-n}$ W m^{-2} where $n = 8, 7, 6, 5$, and 4, for classes A, B, C, M, and X, respectively. Occasionally, flares are observed with peak intensities $\geq 10^{-3}$ W m^{-2}. Although the letters Y and Z were originally for each order of magnitude larger than the X-class, these letters have never been used. Such flares are referred to as X10 events and above, e.g. an X17 or X28 flare (Cliver et al., 2022).

NOAA/SWPC provides charts with the evolution of the GOES X-ray flux over the last 6 hours to 1 week, and has a supplementary webpage that contains specifics on – amongst others – solar flares as observed by GOES.[10]

2.2 "Old" GOES flare statistics

The entire list of flares from the start of the GOES observations until 2017 is available on the website of NOAA/NCEI.[11] In this paper, missing flares from mid-2017 till the end of 2019 (C-, M-, X-class) were added from the "Weekly".[12]

The resulting file covers 77775 flare events for the period January 1976 – December 2019 and is available as a Supplementary data file "Supplementary Data A_GOES flares_Old and New.xlsx". A few incomplete and ambiguous flare entries were eliminated, i.e. 31 flares for which no peak intensity was mentioned and another 175 flares which had "C0" as peak flux. This still leaves 77569 events in the database.

The B-class events are largely underreported because they were only included by NOAA in the reports from 1983 onwards, and they were not counted from the "Weekly" summaries from mid-2017 onwards. Also, at times of high solar activity, the overall soft X-ray background flux can be so high that it overwhelms any B-class and, on occasion, even C-class flares that are being produced (Bornmann, 1990; Ryan et al., 2012). In this paper, as we are focusing on predictions of flares peaking at and above the C1 level and not trying to detect any

[9] The X-ray sensors (XRS) are continuously improved. The current XRS (GOES-16 and higher) are actually taking one measurement every second, whereas the time cadence for the GOES-13-15 was 2 seconds and that for the older GOES generation 3 seconds. (https://www.ngdc.noaa.gov/stp/satellite/goes/ and https://www.ngdc.noaa.gov/stp/satellite/goes-r.html).

[10] The NOAA/SWPC charts with the GOES x-ray flux are at https://www.swpc.noaa.gov/products/goes-x-ray-flux, whereas the solar and geophysical event reports are at https://www.swpc.noaa.gov/products/solar-and-geophysical-event-reports.

[11] NOAA National Centers for Environmental Information (NCEI), which has integrated since 2015 the National Geophysical Data Center (NGDC); the website is at ftp://ftp.ngdc.noaa.gov/STP/space-weather/solar-data/solar-features/solar-flares/x-rays/goes/xrs/.

[12] The Weekly, short for Preliminary Report and Forecast of Solar Geophysical Data, is jointly produced by the National Oceanic and Atmospheric Administration (NOAA) Space Weather Prediction Center (SWPC), and the Air Force Weather Agency (AFWA). They are available online at https://www.swpc.noaa.gov/products/weekly-highlights-and-27-day-forecast (1997 till present), with paper-only versions of the current series of weekly reports starting on 09 September 1975 with serial number PRF 001. Note the solar flare events can also be distilled from NOAA/SWPC daily solar event reports (1996-present) available at NOAA/NCEI ftp://ftp.ngdc.noaa.gov/STP/space-weather/swpc-products/daily_reports/solar_event_reports/.

underlying physical mechanism of solar flares, we have followed Wheatland (2005) and made no attempts to correct or subtract for the soft X-ray background (see also e.g. Leka et al., 2019a; Wheatland & Litvinenko, 2002; McCloskey et al., 2018).

In the NOAA/NCEI database, 44.1% of the reported flares have no source region assigned, most of them (96.8%) belonging to the B- and C-class. Until 2004, locations and flares were linked to each other using optical (H-alpha) observations by the USAF network, after which NOAA started to use GOES imagery (SXI).[13] Thus, certainly prior to 2004 (prior to GOES-12), flares can be missed in optical observations due to e.g. bad weather conditions. Anticipating the calculation of flare rates for the McIntosh classes for this study, we made a special effort to assign a source region to a maximum of flares with a peak intensity of C7 or higher. This was done by checking EUV imagery from SDO/AIA (Lemen et al., 2012) and SOHO/EIT (Delaboudinière et al., 1995), corresponding white light imagery from SDO/HMI (Schou et al., 2012) and SOHO/MDI (Scherrer et al., 1995), and the daily NOAA SWx bulletins (RSGA[14]). Doing so, a source region was retrieved for 692 out of 2109 of the flares concerned. This means that a source region was assigned to 86% of the X-class flares and 44% of the M-class flares that were initially lacking such a source region. That there are still several missing is mostly due because, aside from too little information in the pre-1997 bulletins, sometimes the flare was the result of a filament eruption, or the flare took place behind the solar limb with 2 or more active regions near that location, or there were flare events in different active regions going on simultaneously, making the identification of the source ambiguous.

2.3 "New" GOES flare statistics and comparison

Following the recommendation by NOAA/NCEI for the pre-GOES-16 data (See Footnote 8), all flare peaks in the database ("old" GOES data) were divided by 0.7, i.e. upscaled by a factor 1/0.7 = 1.429. This represents a shift by +0.155 in the logarithmic C-M-X scale. In all that follows, "GOES old" means the events before this upscaling ("old" GOES data), and "GOES new" means the events after they have been upscaled by removing the 0.7 factor ("new" GOES data). The full intensity was used for this upscaling, and then rounded down (e.g. C6.9 divided by 0.7 would become C9.8 and not C9.9). Note that for the flare data since GOES-16 (post 2019), this upscaling is no longer required because the 0.7 factor is no longer applied to the flare's peak intensity by NOAA.

Table 1. The number of flares per GOES X-ray class and per solar cycle, before and after the removal of the 0.7 downscaling factor ("GOES old" and "GOES new", respectively the upper and lower portion of the table). A 50% increase in the number of M-class and X-class events is obvious (respectively 55% and 52%). Solar cycles are from the 13-month smoothed monthly sunspot number minimum to the next minimum (Meeus, 1958), with the data from January to March 1976 added to SC21.

	SC21	SC22	SC23	SC24	Total
GOES old					
A		2	9	2	13
B	2857	6128	8470	5403	22858
C	14487	12439	13162	7736	47824
M	2184	2020	1442	733	6379
X	168	152	126	49	495
Total	**19696**	**20741**	**23209**	**13923**	**77569**
GOES new					
A		1	4		5
B	2216	4713	6423	3888	17240
C	13776	12752	14322	8835	49685
M	3441	3043	2277	1124	9885
X	263	232	183	76	754
Total	**19696**	**20741**	**23209**	**13923**	**77569**

Table 1 shows the number of flares per GOES X-ray class and per solar cycle before and after the removal of the 0.7 downscaling factor (respectively the upper and lower portion of the table). A 50% increase in the number of M-class and X-class events is obvious, with respective percentages of 55% and 52%. This bears on the workload of those forecast centres issuing advisories and warnings to civil aviation and other SWx end users (satellite operators, etc.) whenever a solar flare reaches the X-class level (e.g. Devos et al., 2014; Kauristie et al., 2021). Furthermore, it changes the number of alerts and contingency actions along the entire space weather chain, up to the end users and customers (switching to safe mode for satellite operators, changing band for telecom, etc.). Also, in the solar cycle research domain, there are important consequences, e.g. in the prediction of the number of flares (Janssens, 2021) or in the maximum strength of a solar flare (Cliver et al., 2022). Moreover, for SC25 it may create some wrong ideas about the activity of the ongoing solar cycle. Indeed, the already high number of recorded M- and X-class flares for SC25 – over 1250 until September 2024[15] – is only in part due to the much higher solar activity than initially expected (NOAA/SWPC[16]). Even if the sunspot numbers for SC25 had been similar to that of the previous SC24, then there would still have been a 50% increase in reported M- and X-class flare numbers simply because the 0.7 downscaling factor is no longer applied. This is something to keep in mind when comparing the high flare activity of SC25 with that of its predecessor. There is also an important change in the number of very strong flares (X10 or larger) recorded during the GOES era. Indeed, because of the

[13] From the Read Me file on NOAAs Edited Solar Events list: ftp://ftp.swpc.noaa.gov/pub/indices/events/README and NCEI documentation at https://www.ngdc.noaa.gov/stp/space-weather/solar-data/solar-features/solar-flares/x-rays/documentation/miscellaneous/ as well as at https://web.archive.org/web/20150703131213/http://sxi.ngdc.noaa.gov/.Unlike GOES-12, the subsequent GOES-13 through GOES-15 spacecraft lacked reliable flare location capability due to instrumental issues. So, SWPC returned to using H-Alpha flare locations provided by USAF or mapping the flare to the center of the most likely region responsible for the flare. This practice has continued through the present day. While flare location was restored for GOES-16 onward, this has not been implemented operationally pending verification and validation efforts and algorithm refinement.

[14] RSGA: SWPCs daily Report of Solar and Geophysical Activity, available at ftp://ftp.swpc.noaa.gov/pub/warehouse/ (1966-present).

[15] STCEs Solar Cycle 25 Tracking page: https://www.stce.be/content/sc25-tracking (updated 11 October 2024).

[16] From the international SC25 Prediction Panel: https://www.swpc.noaa.gov/news/solar-cycle-25-forecast-update.

Table 2. The NOAA R-scales with corresponding physical parameter (GOES soft X-ray flare peak intensity), the current average of events per solar cycle as referred to by NOAA, and the calculated averages per SC based on the old data (4 cycles instead of 2) and the rescaled ones. The newly obtained numbers ("GOES new") are closer to the original NOAA averages/SC than the older numbers ("GOES old"), the deviations being respectively 5%–35% and 30%–55%.

NOAA			GOES old	GOES new
R-scale	SXR class	Avg/SC	Avg/SC	Avg/SC
R1	M1–M4	2000	1441	2246
R2	M5–M9	350	154	225
R3	X1–X9	175	118	179
R4	X10–19	8	5	7
R5	≥ X20	< 1	1	2

rescaling, there are now 29 X10–X19 and 8 X20 or stronger events instead of 19 and 3, respectively (Table 2). The most powerful flare in the GOES era is now the X40 from 4 November 2003, instead of X28 as currently reported in the database (same event, but higher intensity as a result of the upscaling).

There are also some interesting effects on the occurrence rates of the five levels of the NOAA's R-scale (see Footnote 2), as described by Poppe (2000). These scales were introduced in the late 1990s to provide a link between a physical space weather parameter, such as the GOES soft X-ray peak flare intensity, and actual observed space weather effects, such as on HF communications. The occurrence rate (number per SC) for each of the five levels of the R-scale (the R stands for Radio blackout) largely overestimated those from an average SC, as they were based on the very active SC21 and 22. However, due to the rescaling effort and the coverage of four full solar cycles, the deviations of "GOES new" numbers of events per SC with respect to the NOAA average SC rates are now within the range 5%–35%, whereas they were in the order of 30%–55% for the "GOES old" numbers (see Table 2). It would be preferable to express these occurrence rates as a function of the predicted/observed amplitude of the solar cycle (see e.g. Janssens, 2021), but this would make it much more difficult to communicate it to the broad public.

3 McIntosh classifications

3.1 Classification technicalities

The McIntosh classification for sunspot groups was introduced by Patrick McIntosh (McIntosh, 1990) in the 1960s. It was an improvement and expansion of the Zürich sunspot classification scheme, which was developed and revised by Max Waldmeier (1938, 1947; Kiepenheuer, 1953), who himself had modified an earlier scheme introduced by Cortie (1901; Carrasco et al., 2015). The general form of the McIntosh classification is Zpc, where Z is the modified Zürich class, p is the type of principal spot, primarily describing the penumbra, and c is the degree of compactness in the interior of the group. These three components can be linked to the magnetic flux, the magnetic flux emergence, and the magnetic topology of the group as outlined by McCloskey et al. (2016). The Zpc scheme results in 60 distinct types of groups, thus allowing for a more detailed description of a sunspot group than the classifications that existed up to that point, all the while keeping the classification process relatively simple for the solar observer.

Figure 1 provides an overview of the different types of sunspot groups, and the various observational parameters that lead to these 60 classes (white boxes). From a basic distinction between unipolar and bipolar sunspot groups, the unipolar groups can be classified according to the presence (or not) of a penumbra around the main spot, and the shape and North-South diameter of the penumbra. The classification of the bipolar groups expands further on this by also considering the distribution of sunspots inside the group, the distance between the two outer main sunspots of the group, as well as which end contains sunspots that have a penumbra (none, one end, or both). Using this table, one can also get a general idea of the outlook of a sunspot group. For example, "Dsc" means a bipolar sunspot region with a length less than 10 degrees, with both ends having a mature penumbra ("D"), of which the largest being symmetrical and small (North-South diameter of less than 2.5°; "s"), but with numerous sunspots between the main spots of which at least one has a fully mature penumbra ("c").

Classifying sunspot groups according to the McIntosh scheme is not always an easy task. In his seminal paper (McI90), McIntosh went to great lengths to meticulously describe the various types and subdivisions of his classification scheme. It contains very precise definitions of what is, for example, a unipolar group, a rudimentary or symmetric penumbra, or an intermediate or compact internal sunspot distribution. Realizing the potential pitfalls for a solar observer when classifying sunspot groups, he devoted an entire section to pointing out difficulties and how to deal with them, warning against assigning a too complex class to a sunspot group, such as for large asymmetric penumbrae.

Several SWx forecast centres, such as the SIDC, MetOffice, and NOAA/SWPC,[17] are using the McIntosh classification in their daily reports and as a step-up for solar flare probability forecasting, with especially the NOAA/SWPC data being easily accessible to the wider community. The sunspot data, including these McIntosh classifications, are reported by NOAA/SWPC in their daily Solar Region Summaries (SRS; see Footnote 7). They have been available for nearly half a century now and constitute a true treasure trove for solar observers, solar researchers, and space weather forecasters. The SRS is a joint product of NOAA and the USAF, which provides a detailed description of active regions observed during the preceding day on the solar disk. It is compiled by SWPC after analysis and compilation of all the individual reports received from USAF's Solar Optical Observing Network (SOON). Determining the best representation of the region's characteristics can sometimes be a challenging task with rapidly evolving regions, and the space weather forecaster must take into account seeing conditions at the individual observatories, the experience of the analysts, and other considerations. On the downside, the SRS inevitably contains

[17] A more complete list is in Leka et al. (2019a; their Table 6), containing also e.g. AMOS (Korean Meteorological Administration and Kyung Hee University), ASAP (University of Bradford) and ASSA (Korean Space Weather Center).

Unipolar				Bipolar													
No penumbra	Penumbra			Sunspot distribution	No penumbra	Penumbra											
Axx				open	Bxo	Penumbra on 1 end			Penumbra on both ends								
				intermediate	Bxi	Length of sunspot group			Length ≤ 10°			10° < Length ≤ 15°			Length > 15°		
North-south diameter main spot	Shape penumbra main spot			Sunspot distribution	North-south diameter main spot	Shape penumbra main spot											
	rudimentary	symmetric	asymmetric			rudim.	symm.	asymm.	rudim.	symm.	asymm.	rudim.	symm.	asymm.	rudim.	symm.	asymm.
≤ 2.5°	Hrx	Hsx	Hax	open	≤ 2.5°	Cro	Cso	Cao	Dro	Dso	Dao	Ero	Eso	Eao	Fro	Fso	Fao
				intermediate		Cri	Csi	Cao	Dri	Dsi	Dai	Eri	Esi	Eai	Fri	Fsi	Fai
				compact						Dsc	Dac		Esc	Eac		Fsc	Fac
> 2.5°		Hhx	Hkx	open	> 2.5°		Cho	Cko		Dho	Dko		Eho	Eko		Fho	Fko
				intermediate			Chi	Cki		Dhi	Dki		Ehi	Eki		Fhi	Fki
				compact						Dhc	Dkc		Ehc	Ekc		Fhc	Fkc

Figure 1. Overview of the different types of sunspot groups and the various observational parameters that lead to these 60 classes (white boxes). From a basic distinction between unipolar and bipolar sunspot groups, the unipolar groups can be classified according to the presence (or not) of a penumbra around the main spot, and the shape and North-South diameter of the penumbra. The classification of the bipolar groups is further subdivided by considering the internal sunspot distribution and the length between the two main portions of the group, and which portion has a penumbra (none, one end, or both).

typos, missing data, misclassification, or bad allocation of NOAA active regions and active region flare assignation. In their effort to produce automated McIntosh classifications, Colak & Qahwaji (2009) produced automated tools to detect inconsistencies in the NOAA catalogues.

Note that the SDO HMI imagery and the recent designation of GONG (Global Oscillation Network Group) imagery as an operational resource now provide additional assessment and monitoring capabilities to the observations provided by USAF. Nonetheless, some errors may remain, as Angryk et al. (2020) pointed out in their effort to provide curated datasets of NOAA active regions and flare catalogues. McIntosh himself was aware of these occasional misclassifications (private communication, 15 November 2004), with Figure 2 providing some examples as illustrations.

3.2 Methodology

In this paper, the McIntosh classification of sunspot groups for the period 1976–2019 was redone, thus covering four full solar cycles and the entire era of the GOES X-ray measurements. It builds on earlier, unpublished work that was started by the lead author in 2005. This explains, in part, the choice for the drawings made by the Kanzelhöhe Solar Observatory,[18] which was one of the databases going back furthest in time with a consistent quality in the solar drawings. The ease of access was also an important factor at that time. The Kanzelhöhe observers are making their drawings using a refractor with a diameter of 11 cm and a focal length of 165 cm. A projection lens then enlarges the primary image to 25 cm diameter and focuses it on an attached drawing plate. Due to the folding of the light path, the drawing is side-reversed (i.e. the east limb is to the right). The solar drawings are made by different observers,[19] with about nine observers having done the bulk of the drawings considered in this paper.

The classifications of the sunspot groups visible in the drawings were made manually, i.e. without the aid of any digital tool. This better mimics the conditions a solar observer would have to deal with. To reduce the workload, about 10 equally spaced observations were selected per month, i.e. about one drawing every 3 days. So, in total, 4720 Kanzelhöhe drawings were evaluated. A quick check based on observations during minimum and maximum years of the solar cycles (965 days), revealed that the median observation time was 08:15UT, with 50% of the observations done between 07:12 and 10:00UT. The median values over the solar cycles are within 15 minutes of this median value, with a slight tendency towards earlier timings over those four decades. Due to the shorter days and lower Sun elevation, the observations during winter (December, January and February) are done almost 2 hours later than during summer (June, July and August), with median values respectively of 09:15UT and 07:20UT. Spring and autumn have observation times close to the overall median values (respectively 08:00UT and 08:05UT).

The McIntosh classifications for each of the recorded sunspot groups on the drawing were added to the NOAA solar data tables. These tables were originally available from the NASA/Marshall Solar Physics website, but then relocated to the Solar Cycle Science webpage[20] in 2017, where they are still available and supplemented with the latest data. During this transition, the McIntosh classification (NOAA/USAF network) was added to the sunspot group data, going back all the way to 1982. While making the McIntosh classifications for this study, these NOAA/USAF classifications were hidden from view to avoid any influence on the author.

[18] Kanzelhöhe Observatory: http://cesar.kso.ac.at/ , with the solar drawing archive at http://cesar.kso.ac.at/synoptic/draw_years.php and a description of the observational set-up at http://cesar.kso.ac.at/instruments/sonne_zeichnungen_en.php#topic2.

[19] A regularly updated overview chart is at http://cesar.kso.ac.at/tmp/observer.png.

[20] NASA/MSFC: https://solarscience.msfc.nasa.gov/greenwch.shtml; Solar Cycle Science webpage: http://solarcyclescience.com/activeregions.html; Note that during this transition also the timing got corrected. Previous date/times were off by a half day. Times were changed from 0.500 days to 0.000 days and dates were incremented by one day.

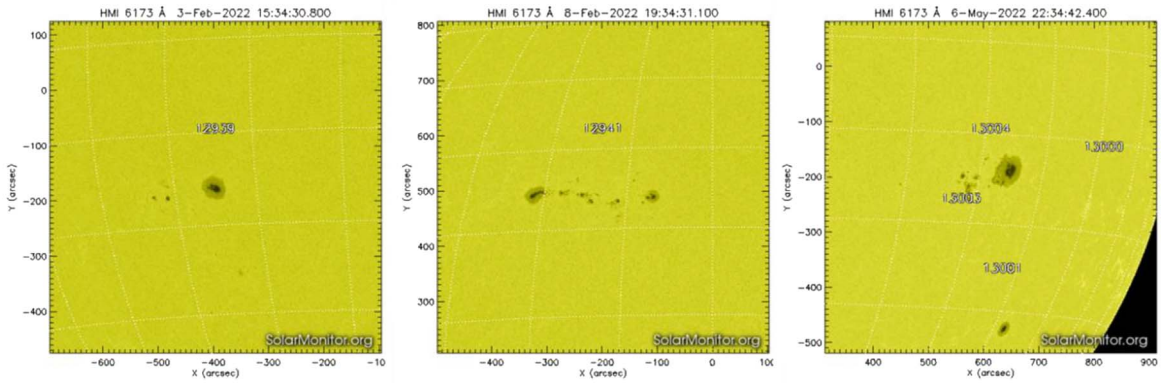

Figure 2. SDO/HMI images with an overlaid 10° × 10° grid as available at SolarMonitor: https://www.solarmonitor.org/, showing a zoom of some sunspot groups that appeared early 2022. NOAA/SWPC classified active region (AR) 12939 as a Dho group, AR 12941 as an Eki group, and AR 13004 as Dkc. Note the McIntosh definitions for a symmetric spot ("s" or "h") allow for an elliptical or slightly irregular penumbra. For the compact sunspot distribution ("c"), at least one mature spot is required between the two main portions. Consequently, more accurate classifications of these 3 groups would have been Cso, Fsi and Dho. The original misclassifications indicate group types with very high probabilities on M- and X-class flares. Consequently, they largely overestimate the actual flare probabilities associated with the more accurate revised classes. Indeed, during the next 24 hours, each of these groups produced only 1 C-class flare.

The location of the sunspot groups mentioned in the NOAA solar data tables greatly facilitated connecting the sunspot groups appearing on the Kanzelhöhe drawings with the corresponding NOAA numbers of the sunspot groups. When a sunspot group mentioned in the NOAA tables was not visible in the Kanzelhöhe drawings, e.g. because it had rounded the west solar limb, then a "0" was inserted. Vice versa, when there was a sunspot group on the drawings which was not mentioned in the NOAA tables, then a new number was created with the structure "Kyynnn", with K from Kanzelhöhe, yy indicating the year and nnn the number of the new group for that year. The very large majority of these groups (83%) concerned small groups (Axx, Bxo, and the smaller H-type groups). The larger groups are mostly concerned with groups split off from more complex regions or occasional NOAA/USAF misses. For the 627 days with a spotless Sun, a "0" was inserted for the McIntosh classification.

The final list contains 22232 genuine (i.e. non-zero) McIntosh classifications for 4720 observing days, available as Supplementary data in the file "Supplementary Data B_McIntosh classifications.xlsx". The Fro class was not observed. Of course, it is very likely that this list will contain some errors and debatable classifications too, despite it being compiled by one "observer" and based on a set of solar drawings that originate from the same institute (Kanzelhöhe). Indeed, the Sun regularly produces sunspot groups that pose a challenge to get accommodated in one of the 60 McIntosh classes, and sometimes, the sunspot groups evolve very fast from simple to complex configurations in much less than 24 hours, allowing for multiple McIntosh classifications for a sunspot group in a single day. While occasional errors should not be a big problem for the statistical analysis, it becomes a problem if there is a certain tendency in the errors such as e.g. a systematic bias towards classifying regions as too complex, or when it affects McIntosh classifications which are relatively rare and thus may quickly affect the flare rate corresponding to that McIntosh class. While classifying the sunspot groups, the authors have put a substantial effort in remaining as close as possible to the original definitions of the Zpc-scheme crafted by Patrick McIntosh, thus avoiding as much as possible any systematic bias.

3.3 Comparison of results

Comparison of the obtained classifications in this paper with the original McIntosh results (Kildahl, 1980; McI90),[21] reveals there is a close match (*z*-test) for all three parameters (Table 3). For the Z-component, the new results have a bit less B-types (14% vs. 18%) than McI90, but a slightly higher percentage for C- and H-types (42.3% vs. 39.9% combined). For the p-component, there is a somewhat larger difference of 7% for the r-type (14.1% vs. 7%), but about 4% fewer sunspot groups without penumbra, i.e. the x-type which corresponds to the A- and B-types (34.5% vs. 38.3%). These small differences can easily be explained by considering the very detailed drawings made by the Kanzelhöhe observers, often showing very puny penumbra around a spot. This naturally results in more Cro, Cri and Hrx types compared to McI90 (11.7% vs. 5.9%). The values for the c-component are nearly identical. Also, the subgroupings are very good, e.g. the percentage for the -kc types is identical to the one mentioned in McIntosh (1.5%).

Comparing the numbers in this and the McIntosh paper with the SWPC data, as mentioned in BL12, reveals significant (*z*-test) differences. An important consideration to make first is that the SWPC values in the BL12 study are limited to the period December 1988 – June 1996, i.e. the maximum and declining phase of solar cycle 22 (SC22), which was a very

[21] Two errors in the McIntosh numbers (McI90) were corrected, based on the numbers in the Bloomfield et al. (2012; BL12) paper: Cri and Cso. In the BL12 paper, 6 classes are apparently missing: Eri, Ero, Fro, Esc, Fac and Fsc (zero counts or no flares reported). Correcting gives the total number of classifications of 12411 as quoted in the McIntosh paper.

Table 3. Percentages of the various subtypes of each of the three components Z, p, and c. The numbers reported are the ones derived in this paper (JJ), from the original McIntosh paper (1990; Kildahl, 1980), the SWPC values for the period December 1988 until June 1996 ("SWPC"; Bloomfield et al., 2012; henceforth BL12), and a portion of the data in this paper pertaining to the same period as SWPC ("JJ_88_96"). All numbers are percentages, except the last line, which represents the total number of classifications made in the respective studies.

	JJ	McIntosh	SWPC	JJ_88_96
Z				
A	20.2	20.3	14.7	21.8
B	14.3	18.0	17.8	14.7
C	19.7	19.1	21.3	20.0
D	15.6	15.5	18.0	15.1
E	5.9	4.9	8.8	5.1
F	1.7	1.3	3.4	1.7
H	22.6	20.8	16.0	21.7
p				
a	13.3	11.6	27.6	12.5
h	4.1	4.0	1.5	4.0
k	4.7	5.1	9.8	5.4
r	14.1	7.0	6.1	14.1
s	29.4	33.9	22.4	27.6
x	34.5	38.3	32.5	36.4
c				
c	2.7	2.4	1.4	2.6
i	15.7	16.5	9.7	15.0
o	38.8	40.0	58.1	39.0
x	42.8	41.1	30.7	43.4
kc	1.5	1.5	1.4	1.7
Total	22232	12411	18733	5237

active solar cycle. The McIntosh values (Kildahl, 1980) concern the period 1969–1976, i.e. the maximum and declining phase of solar cycle 20 (SC20), which was considerably less active than SC22 by about 25% (maximum smoothed sunspot numbers[22] of respectively 156.6 and 212.5).

Therefore, in order to minimize any effect from the difference in strength between the solar cycles, the portion between December 1988 and June 1996 was extracted from our database, and the percentages of the Z-, p-, and c-components were recalculated (column "JJ_88_96" in Table 3). The percentages of the McIntosh classes for this portion of SC22 differ very little from the general average as determined for all 4 solar cycles. Thus, the differences with the SWPC remain obvious: SWPC has 10 to 12% fewer unipolar groups (A- and H-types) than McI90 and this paper, 19–21% more asymmetric penumbra groups, and 18–19% more sunspot regions with an open distribution. This suggests that for the p-component, at least during that period, sunspot groups with a rudimentary or slightly irregular penumbra were considered as having an asymmetric penumbra.

[22] The amplitude for the solar cycles can be found at the SILSO (Sunspot Index and Long-term Solar Observations) webpage: https://www.sidc.be/silso/cyclesminmax All sunspot numbers used in this study are version 2 (Clette et al., 2014).

The differences in the Z- and p-components allude to a reporting problem. Indeed, checking the currently available McIntosh classifications in the Solar Cycle Science database (see Footnote 20), numerous non-existing and thus incorrect classifications can be found. As an example, on 17 August 1989, one can find the following erroneous classifications: Hao, Axo, Ckc, Hho. These should have been Hax, Axx, Cki and Hhx. These NOAA/USAF lists also contain a lot of doubles, i.e. on 18 August 1989 there were 2 entries for NOAA 5643 and 5645. The final list created for this research contains 512 doubles, which were given a special number starting with D to indicate that this was a double. Of these double-counted groups, 65% were reported between December 1989 and June 1996, 75% were given the McIntosh class "0", and the remainder were very simple groups such as Axx, Bxo, and Hrx. It is unclear if BL12 took these errors and anomalies into account when compiling their list with region counts per McIntosh class (their Table 2, columns 1 and 2), but it may explain at least in part the previously mentioned anomalies in the Z, p, and c classes, and thus also affect the flare rates. It is also noteworthy that the percentage of compact groups ("c") is only half that of established in McI90 and this paper. This seems to be the reverse of what has been observed in the SWPC data during the most recent solar cycle 24 (SC24), where there seems to be a tendency to over-assign complex classifications, as illustrated in Figure 2.

4 Flare rates and flare probabilities

4.1 Methodology and results

Merging the flare list (Sect. 2) with the sunspot group list (Sect. 3), a new list is compiled containing year, month, day, NOAA group number, McIntosh classification of each group, and the number of C-, M- and X-class flares produced by that group for that day. As the bulk of the Kanzelhöhe observations were done during the morning hours, the McIntosh classes were considered valid for the entire day (so from 00 UT onwards). In other words, counted flares can have occurred either before or after the time of the Kanzelhöhe drawing on the same day, but mostly after, given that the drawing time usually falls early on the UT day. That way, the flare numbers could be summed for that day (00-24UT), thus avoiding a laborious check consisting of determining for each observing day at what time the Kanzelhöhe observation was done and then scrutinising all the flares for the next 24 hours. The newly obtained list contains 10202 flares (7653 C-, 2351 M- and 198 X-class events) distributed over 22232 groups with a McIntosh classification.

The Supplementary file "Suppl Mat_Results A_McI counts_upscaled(GOESNew)flarerates" tabulates for each McIntosh class the counts, the total number of flares associated with it (C, M, and X), the flare rate over 24 hours and the error following the methodology outlined in BL12. The next three columns represent the flare rate over 24 hours for C+ flares (C1 or higher flare, so summing for C- and M- and X-class flares), for M+ flares (M1 or higher flare, so summing for M- and X-class flares), and for X+ flares (the same as for X flares). The last columns are the error (BL12) and the McIntosh class again, which were added to guide the eye.

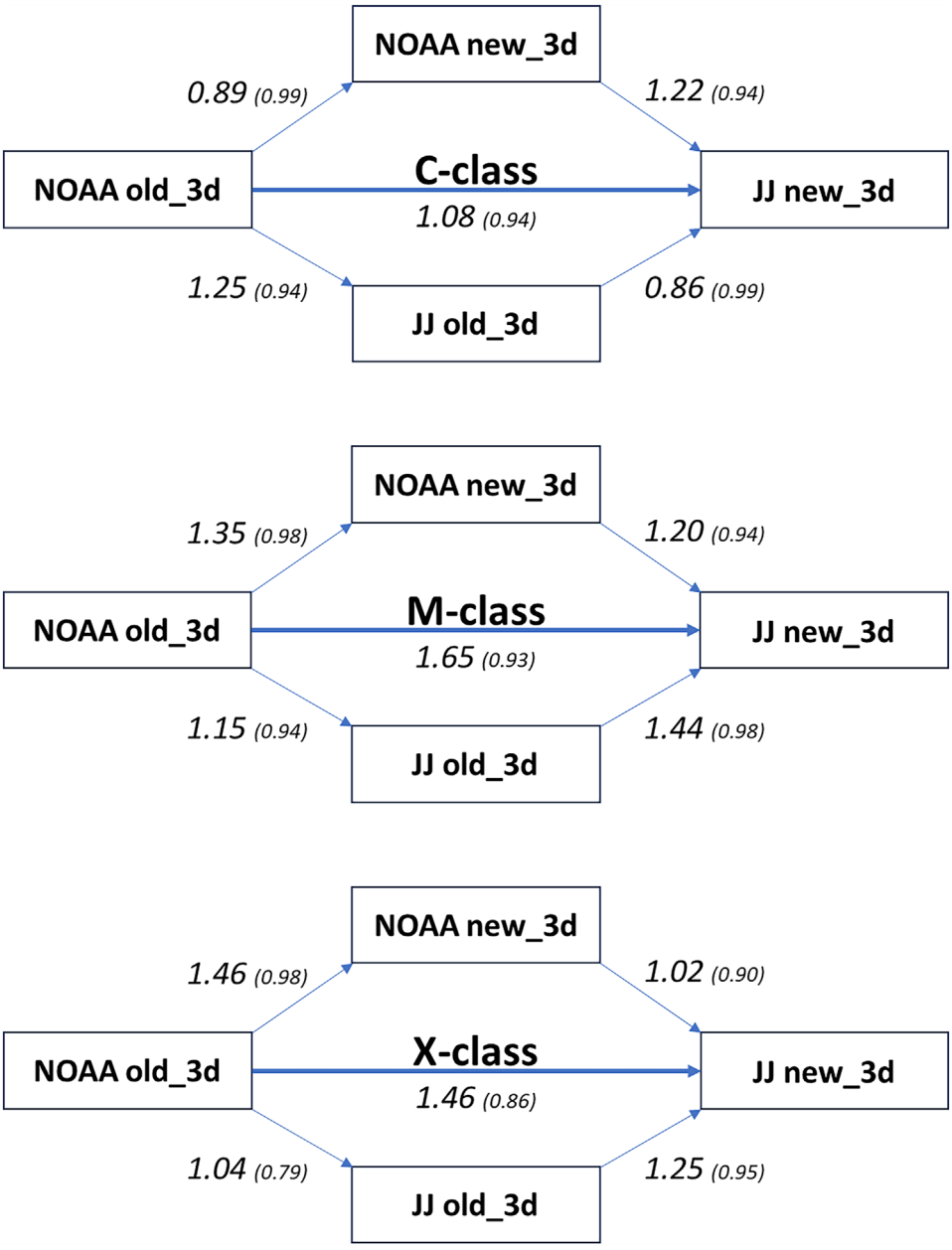

Figure 3. In order to have an idea of the individual impact by the flare upscaling and the redoing by the McIntosh classifications, the correlation between four lists with flare rates (1988–1996) was calculated providing the slope and correlation coefficient r (between parentheses) obtained by a linear regression forced through the origin. The four series are the McIntosh classifications in this paper with GOES old and GOES new flare counts (resp. JJ old 3d and JJ new 3d) and the NOAA McIntosh classifications with GOES old and GOES new flare counts (resp. NOAA old 3d and NOAA new 3d). The suffix "3d" is to emphasize it concerns classifications done on average every 3 days. All regressions have a p-value < 0.0001. A further discussion is in the text.

Given the flare rates for C+, M+, and X+ categories, and assuming that flares are occurring following a Poisson distribution, the probability of having at least one flare of C+, M+, X+ category can be computed, as well as a confidence interval on these probabilities, as explained in Appendix.

The Supplementary file "Suppl Mat_Results B_Flare probs_confidence intervals" tabulates for each McIntosh class the counts, the number of C+, M+ and X class flares, and then for each of these three categories the Poisson flare probability and the corresponding confidence intervals (low, high). These probabilities are used by SWx forecast centres such as the SIDC.

4.2 Comparison with previous studies

Comparing the flare rates for the McIntosh classes reported in this paper with those in BL12, there is a generally good correspondence in the sense that the most complex sunspot

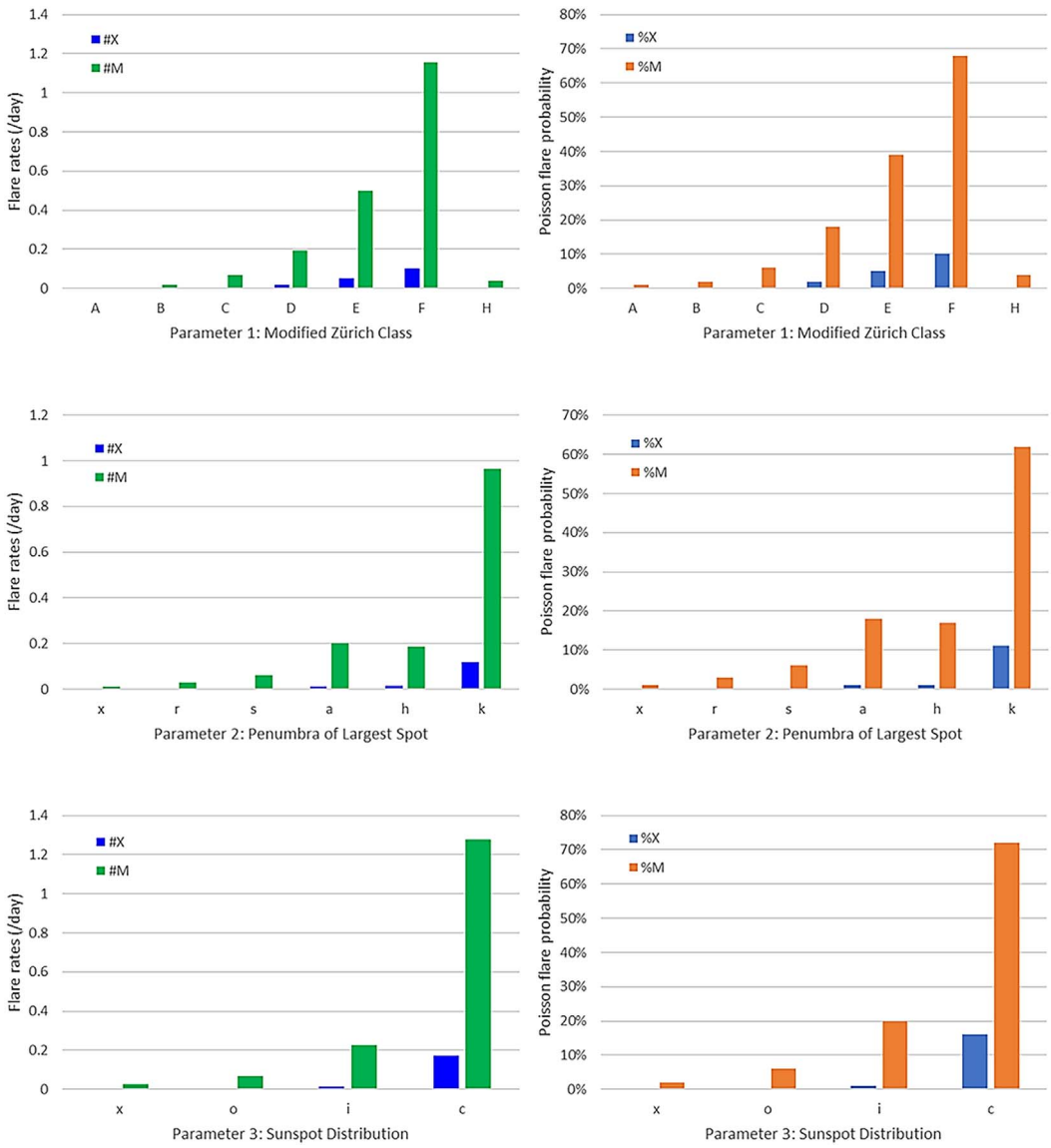

Figure 4. M- and X-class flare rates (#/day) and Poisson flare probabilities (%) for the individual components of the McIntosh classification. A discussion of the results is provided in the text.

groups produce the most flares. Because of the upscaling of the GOES flare intensities performed in our paper ("GOES new"), the flare rates mentioned in BL12 are generally lower than those in the Supplementary file "Suppl Mat_Results A" for C-class flares (slope of 0.81; correlation coefficient $r = 0.95$), M-class flares (0.69; $r = 0.93$), and X-class flares (0.79; $r = 0.86$). Note that these values were calculated through a linear least-squares regression forced through the origin, and with only 48 of the 60 possible classes: 6 were missing in the BL12 table (their Table 2) because no counts and/or no flares were observed, whereas six McIntosh classes were removed because there were large dispersions in one or more of the three flare classes (C, M, X) due to the small numbers (counts) of flares involved. A single flare-active (or inactive) sunspot group can then make a big difference in flare rates for that particular McIntosh type. This was the case for McIntosh types Fsi, Ehc, Fhc, and Fri. For Dsc and Dri, the anomalous rate for C-class flares compared to this paper (respectively 0.00 vs 1.29, and 3.50 vs 0.47) is thought to be caused by the artificial computation of the number of C-class flares as outlined in the BL12 paper. Indeed, Kildahl (1980) did not provide the number of C-class flares that could be used for the BL12 study. Thus, in order to provide C-class-related forecasts comparable to those for M- and X-classes, flare rates measured over 1988–1996 by NOAA were assumed to hold for 1969–1976. The relative numbers of McIntosh observations in the time periods were then used by BL12 to determine the expected number of C-class flares for 1969–1976. Thus, if the NOAA C-class flare rates were off, it would explain the large difference in the C-class flare rate between BL12 and this paper.

Evaluating the flare rates in this work compared to the BL12 paper for all 3 flare classes (C, M, X) and all McIntosh types for which flare rates were available (54 types for 3 flare classes), an increase was found in 62% of the cases (100 of 162), 21%

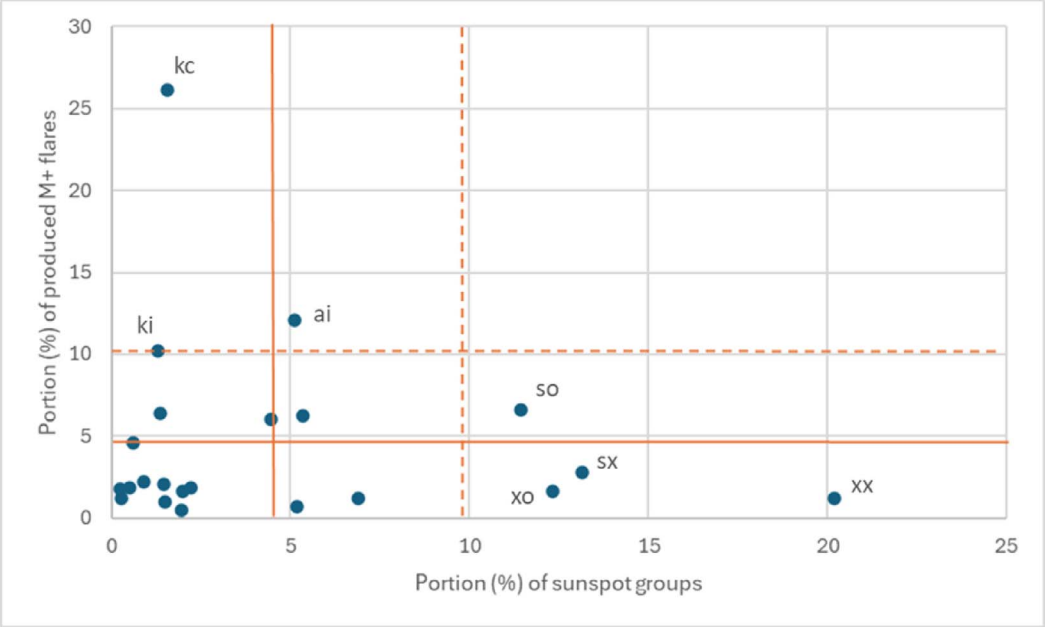

Figure 5. For the 22 possible combinations of "p" and "c" (last 2 components of the McIntosh classification scheme), this graph shows on the horizontal axis the % of these groups of the total number of classified sunspot groups (22232) and on the vertical axis the % of M- and X-class flares (2549) they produced. The full orange and dashed orange lines represent, respectively, the average and the average + 1 standard deviation. 57% of all groups produce only 12% of all M- and X-class flares (4 "pc" types in the lower right), but 48% of all M- and X-class flares are produced by just 8% of all groups (3 "pc" types in the upper left). More details are provided in the text.

showed a decrease, and for 17% the same rate was reported than the one in BL12. A more pronounced smaller flare rate (difference with BL12 > sigma) was found only for 13 McIntosh types and concerned mostly sunspot groups with a symmetric penumbra (10 types), often associated with an intermediate ("i") sunspot distribution. A significantly higher flare rate (difference with BL12 > sigma) was found for 55 McIntosh types and concerned mostly McIntosh group types with an asymmetric penumbra (34). Of note is that for the X-class flare rate, the differences with BL12 were much smaller. Only the Dkc class had a significantly higher flare rate than BL12 (+0.15/day).

4.3 Individual contributions

The flare rates reported in this paper are, in general, higher than the ones reported in BL12. It should be clear that a direct one-to-one comparison is not possible, and that there will always be a difference in flare counts, McIntosh counts and associated flare rates between this paper and e.g. BL12. Indeed, the NOAA data used in BL12 run from 1988 to 1996 (daily observations, old GOES) BL12 combines NOAA's 1988–1996 data with Kindahl's (1969–1976; daily observations, pre-GOES), whereas the classifications and counts in this paper run from 1976 to 2019 (new GOES) with on the average one observation every 3 days. The ideal way to disentangle the two effects (GOES flare upscaling, updated McIntosh counts) on the flare rates would be to have a day-per-day, group-per-group comparison. However, the NOAA and Kindahl source data used in BL12 are not available.

So, in order to get a rough idea on how much the GOES flare upscaling and the redoing of the McIntosh classifications individually contribute to these higher flare rates, a specific project was initiated for the period December 1988 – June 1996, i.e. the same period covered in BL12 for the NOAA data. For this period, the McIntosh classifications from NOAA were taken from the Solar Cycle Science webpage (see Footnote 20) but only for the days that were "observed" in this paper (i.e. on the average every 3 days). For those days and McIntosh counts, the link was then made to the "old" and "new" number of GOES flares. That gives four series for which the flare rates can be calculated: McI in this paper with GOES old and GOES new flare counts (resp. JJ old 3d and JJ new 3d); NOAA McI with GOES old and GOES new (resp. NOAA old 3d and NOAA new 3d). Note that the obtained flare rates will still differ from BL12 because (1) they included the Kindahl numbers (1969–1976), and (2) looking only at the NOAA portion of BL12, the NOAA data are the *daily* classifications for that period. It is not possible to do the McIntosh classifications for every day between 1988 and 1996, as aside from the excessive workload, the Kanzelhöhe Observatory has no drawings for cloudy days, hence a one-on-one daily equivalent from NOAA is unfeasible.

The 1988–1996 NOAA data taken from the Solar Cycle Science webpage contain 21871 entries, of which 1880 were immediately eliminated because they were doubles of a group (within the same day), as discussed in Section 3.3. They were recognizable by the suffix A, . . ., H following the NOAA group number. Most (87%) of these removed groups had a sunspot area of 0 or 10 MH, and the related NOAA group (without the suffix) usually had the largest sunspot area or most complex

McIntosh classification. From the remaining 19991 classifications, 7293 had a non-existing McIntosh class. These concerned mostly (96%) Axo, Hao, Hro, and Hso types and were subsequently converted to the most likely classification, e.g. Axx, Hax, Hrx and Hsx. Also, here, the concerned groups had very small areas. The Ckc types were the only somewhat more complex groups with a large sunspot area, which were, after some closer examination of the Kanzelhöhe drawings, assigned to Dkc or Cki. This list was then combined with the GOES flare list and the McIntosh list from this paper.

For every flare class (C, M, and X), the correlation between the four lists with flare rates was then examined, as shown in Figure 3. There are two ways to go from NOAA old_3d to JJ new_3d. On the first path, one can start by checking the impact on the flare rates from moving from the "old" to "new" (upscaled) number of GOES flares and then the impact from the differences in a number of McIntosh classifications from NOAA to JJ. This is the path NOAA old_3d => NOAA new_3d => JJ new_3d. The other path first examines the influence on the flare rates by the changes in the number of the McIntosh classifications from NOAA to JJ (old GOES), followed by the impact on the flare rates from moving from the "old" to "new" (upscaled) number of GOES flares. This is the path NOAA old_3d => JJ old_3d => JJ new_3d.

For each of the transitions, Figure 3 provides the slope and correlation coefficient r obtained by a linear regression forced through the origin and with data based only on those McIntosh classes with 10 or more classifications, i.e. leaving 35 to 43 data points depending upon the examined flare rate lists. All regressions have a p-value < 0.0001.

For the C-class flare rates, the mild increase (slope of 1.08) is especially due to changes in the McIntosh classifications (NOAA => JJ; 1.22–1.25), whereas the GOES flare upscaling (old => new) actually brings the slope of the flare rate down a bit (0.86–0.89; possible reasons outlined in Sect. 2.2). For the M-class flare rates, the significant increase in flare rate (1.65) is due to strong contributions from both the changes in McIntosh classifications (1.15–1.20) as well as from the flare upscaling (1.35–1.44). The X-class flare rates also show an important increase (1.46), but this is mainly due to the effects of flare upscaling (1.25–1.46). The changes in McIntosh classifications have a much smaller impact (1.02–1.04).

4.4 Comparison of individual components

The graphs in Figure 4 provide the M- and X-class flare rates (#/day) and Poisson flare probabilities (%) for each of the 3 individual components of the McIntosh classification. A comparison with the graphs in McI90 (his Figure 3, flare rates) reveals that these graphs are only differing in detail. They confirm that large and complex sunspot groups are the most flare-active and that the McIntosh classification allows to distinguish these regions. Sunspot groups with an intermediate sunspot distribution or a symmetric main spot lose somewhat in flare rate in favour of sunspot groups with a compact sunspot distribution or an asymmetric main spot. Note that the McI90 flare rates are actually those from Kildahl (1980) as can be calculated from the BL12 paper. Considering the period covered (1969–1976), the flare measurements have been made by the SOLRAD satellite and thus are a priori not susceptible to the scaling issue as discussed in Section 2 (see also Kahler & Kreplin, 1991). This explains the little difference between the flare rates for the individual Z, p, and c-components reported in this paper and those in the McI90 paper. Only for the individual E- and F-components, the Kildahl X-class flare rate is remarkably higher than those reported in this paper, most likely due to the high number of X-class flares reported in this period (141 during the 1969–1976 period). The M- and X-class flare rates that can be calculated for NOAA/SWPC based on the BL12 data show an average deficit of 20 to 30% compared to those reported in this paper. Aside from that the period covered here being different (1988–1996), the downscaling issue (Sect. 2) here dominates the numbers. As such, the flare rates reported in the BL12 paper are thus based on McIntosh classifications from 2 different observer teams and during two different periods, and on X-ray measurements taken by two different satellites.

Similar conclusions can be drawn from a comparison of the flare probabilities with the Gallagher et al. (2002) paper (their Fig. 4, flare probabilities). The resemblance between the graphs is very good, with the main difference that most numbers are significantly higher than those from Gallagher et al. This is particularly true for the more flare-productive McIntosh components such as E/F, h/k, and c, where the probabilities are twice as high. For a large part, this is due to the effect of the GOES X-ray flux 0.7 rescaling (see Sect. 1: 50% more M- and X-class flares), but there may also be effects from the different periods that are considered (different overall levels of solar activity) as well as from a difference in classifications. Indeed, Gallagher et al. used the NOAA/USAF data for the period between 1988 and 1996 (with almost no X-class flares ("old GOES") from 1993 to 1995), while differences in McIntosh classifications are present between this study and NOAA/USAF, as pointed out in Section 3 (Table 3).

The fact that large and complex sunspot groups have higher flare rates can also be illustrated by focusing on the last two parameters of the McIntosh classification, i.e. "p", representing the presence, shape and size of the penumbra of the main sunspot, and "c", the compactness of the sunspot distribution inside the sunspot region. "pc" thus results in 22 possible combinations, for which we can compute both the portion in the total of sunspot groups (22232) and the number of M- and X-class flares they have produced (% of 2549 M- and X-class flares; "new GOES"). The result is shown in Figure 5, with the horizontal axis displaying the percentage of sunspot groups and the vertical axis the percentage of M- and X-class flares that they produced. The full orange lines represent the average percentage, and the dashed orange lines represent the average value +1 sigma. The "average +1 sigma" values for both parameters, i.e. the portion of sunspot groups and the portion of produced M- and X-class flares, end up being around 10% of the respective totals.

Interestingly, only a few "pc" combinations have higher values than this 10%. As it turns out, the four datapoints in the lower right of Figure 5 combine to 57% of all sunspot groups but produce only 12% of all M- and X-class flares. These are the McIntosh classes ending in -so, -sx, -xo and -xx, which belong to the smallest and simplest sunspot regions, i.e. they only reached a minor extent or marked the initial emergence and final decay stages of larger sunspot groups

(Axx, Bxo, Hsx). On the other hand, the three datapoints in the upper left of Figure 5 are responsible for the production of 48% of all M- and X-class flares, yet they constitute only 8% of all sunspot groups. These are the McIntosh classes ending in -ai, -kc, and -ki, representing sunspot groups with an asymmetric main spot and a more complex (intermediate or compact) internal sunspot distribution. The remaining 35% of the sunspot groups (15 "pc" combinations) is responsible for 39% of the M- and X-class flare production.

Though the McIntosh classification is a great tool to forecast flare activity, there remain large differences in the actual flare behaviour of individual sunspot groups within the same class. As an example, of the 104 Fkc groups in this study, there were still 30 cases with no M- or X-class flare produced during the subsequent 24 hours. In 7 cases, groups associated with this McIntosh class did not produce any flare at all. Respectively, 67% and 86% of these zero-flare Fkc groups date from before 1996 (pre-SOHO/SDO era), suggesting that this is – at least in part – related to reporting problems within the NOAA/USAF network (bad weather conditions, etc.). Another factor may be that some of the classifications in this study may be wrong, or at least debatable, especially in cases close to some of the limits that the Zpc system imposes, such as the length of the group (e.g. 10° or 15°), or the North–South diameter of the main spot (2.5°). These errors are thought to be minimal in this paper due to the overall close agreement of the results to those presented in the original McIntosh paper.

4.5 Evolution of the sunspot group morphology

As mentioned earlier in Section 1, SWx forecasters facing this flare productivity dilemma try to fine-tune their flare forecasts by looking at other parameters. An important parameter to consider is the evolution of the sunspot group morphology, as outlined by McCloskey et al. (2016, 2018). Studying the daily evolution of the McIntosh class and linking this to the flare productivity of the group, they concluded that sunspot groups increasing in Zürich, penumbral, or compactness class over 24-hour timescales have systematically higher flare rates than those showing no change in these classes. Note that the flare rates mentioned in the McCloskey studies would have been generally higher if the GOES rescaling effect was taken into account, as outlined in Section 2.

Thus, in an exploratory study of our data, we linked the McIntosh classification and flare production for a sunspot group on a given day (day "d") with the next, new classification and flare production of that sunspot group, usually 3 days later (day "d + 3"). Our preliminary results confirm the McC16 and the Lee et al. (2012) findings, namely that – within the same McIntosh component Z, p, or c – the accumulated flare rates are higher or lower when the sunspot region is respectively in a developing mode (larger and/or more complex) or in a decaying mode (smaller and/or simpler) compared to when the region remains the same. The overall flare ratios for the ≥M1 flare rates are respectively about 2.5 for positively evolving components and 0.4 for negatively evolving components compared to the non-evolutive rates. Though this is a reasonable result, we elected – for this paper – to not investigate this topic any further. The main reason is that there are about 3 days between two consecutive classifications (Sect. 3.2, Paragraph 2). Over such a time period, the McIntosh classification can evolve into a much wider variety of other McIntosh classes than in the shorter 1-day interval used in McCloskey, in particular if the group is evolving quickly. This limits the accuracy of the obtained results and increases the uncertainties in the deduced flare rates/probabilities in each category.

The encouraging result of our preliminary analysis suggests taking up a specific, more detailed study, perhaps not only for a 1-day delay but allowing for a range of delays to match daily gaps typically found in individual ground-based solar series. This would require a more extensive, multi-station standardized sunspot group catalogue, which can then be used in future work. In this context, we want to mention "DigiSun"[23] which is a software developed at ROB to measure the parameters from scanned sunspot drawings and save them in an external database. One important application is the study of the evolution of physical variables (area, tilts, heliographic position, etc.) in the long term to constrain dynamo models and better understand the solar cycle. Initially developed in 2011, it recently was completely rewritten with new functionalities such as the area measurement. One of the strengths of the software is its ability to handle different drawing formats and hence to analyze drawings from other collections. By sharing the software with different observatories, the plan of the ROB/SILSO team is to achieve a better homogenization of solar data. This would ease the merge of the data from different collections to fill the inevitable data gaps at one single station and extend the collection back to the past. A first successful international collaboration with the Specola Observatory in Locarno was initiated in 2019, and since then it is used there to analyze the daily sunspot drawing. The Taipei Observatory will use it to analyze its sunspot drawings in 2023, and the Kandili Observatory will install it to analyze their daily drawings.

5 Conclusions

Following NOAA's recent changes in determining flare intensity from GOES observations, the old flare intensities were rescaled by eliminating the 0.7 downscaling factor, as recommended by NOAA. This led to an increase of 55% and 52% in the number of M-class and X-class events respectively. There are now also 29 X10–X19 and 8 X20 or stronger events, instead of respectively 19 and 3 previously. The events per SC based on the rescaled flare numbers now conform much better to the occurrence rates currently given in NOAA's R-scale.

This paper has amply illustrated the importance of a correctly applied McIntosh classification. For the period covering 1976–2019, 4720 Kanzelhöhe solar drawings were visually evaluated and the McIntosh type of 22232 sunspot regions was determined. There is a close match for all three McIntosh components with the results reported in the original McI90 paper. Some small differences, in particular for sunspots with a rudimentary penumbra, can easily be explained by considering the very detailed drawings made by the Kanzelhöhe observers, often resolving very small penumbrae.

On the other hand, rather large differences were found with the classifications by NOAA/USAF during the period 1988–1996. Compared to both the McI90 results and our study, the

[23] The DigiSun webpage is at https://sidc.be/users/sabrinabct/digisun/digisun.html.

SWPC catalogue has about 12% fewer unipolar groups (A and H), almost 20% more asymmetric penumbra groups, and about 20% more sunspot regions with an open distribution. These deviations are thus specific to the SWPC data and in the NOAA database and seem to be due to a systematic bias from the original McIntosh definitions as well as some misclassifications.

Our study, as far as we know, the first to do so, provides a list with the newly calculated flare rates ("Suppl Mat_Results A") and a list with flare probabilities and corresponding confidence intervals ("Suppl Mat_Results B"), based on the updated GOES flare list and the redone McIntosh classifications over the period 1976–2019. Due to the rescaling of the GOES flare intensities, the flare rates mentioned in BL12 are generally lower than those derived in this paper by about 15–30%. Somewhat smaller flare rates were obtained for sunspot groups with a rudimentary or symmetric penumbra, often associated with an intermediate sunspot distribution. Somewhat higher values were mainly found in McIntosh group types with an asymmetric penumbra, often associated with a compact sunspot distribution. The flare probabilities derived in this paper for the more flare-productive components, such as E/F, h/k, and c, are about twice those mentioned in the Gallagher et al. (2002) paper (their Fig. 4), in large part because of the GOES X-ray flux rescaling. However, the differences result also partly from the different time periods of their source data, as well as from a difference in classifications. By avoiding the inhomogeneity of the classifications used in those earlier studies and using homogeneous GOES fluxes scaled to the current GOES-16 daily data, our new results thus deliver a better statistical set of flare rates and probabilities per McIntosh class.

An examination of the respective impact from the flare upscaling and the updated McIntosh classifications on the flare rates revealed that both have important contributions to the M-class flare rates. The increase in C-class flare rates is mostly dominated by the influence of the redoing of the McIntosh classifications, whereas the increase in X-class flare rate is mostly dominated by the effect of the flare upscaling.

The McIntosh classification is very successful in distinguishing flare active from flare inactive regions. This is also clear when considering only the "p" and "c" components of the McIntosh classification, i.e. from the analysis of the same number of flares used in the flare rate calculations but distributed now over only 22 "pc" combinations instead of the 60 McIntosh classes. Overall, we find that 48% of all M- and X-class flares in our study are produced by only 8% of all sunspot groups belonging to the McIntosh classes ending in -ai, -kc, and -ki. For example, the -kc subclass represents only 1.5% of the 22232 assigned McIntosh classifications, yet these groups were the source of 26.2% of the 2549M- and X-class flares. The -ai, -kc, and -ki subclasses correspond to sunspot groups with an asymmetric main spot and a more complex (intermediate or compact) internal sunspot distribution. About 57% of all classified sunspot groups produce only 12% of all M- and X-class flares. They belong to the McIntosh classes ending in -so, -sx, -xo and -xx, which correspond to the smallest and simplest sunspot regions and the phases marking the emergence and final decay of sunspot groups (Axx, Bxo, Hsx). The remaining 35% of the sunspot regions (15 "pc" combinations) is responsible for 39% of the M- and X-class flare production. Here, it concerns mostly small, moderately complex groups (-si, -sc, -hi, -hc, etc.) and somewhat larger, but relatively simple regions (-ho, -ko, -hx, -kx, etc.). Though the McIntosh classification is a great tool to forecast flare activity, there remain large differences in the actual flare behaviour of individual sunspot groups within the same McIntosh class. As an example, our study found that of the 104 Fkc groups, there were still 30 cases with no M- or X-class flare produced during the subsequent 24 hours.

In future work, it is considered to apply digitization software such as DigiSun on large collections of sunspot drawings from several institutes. From these results, the impact of the evolution of the sunspot group can then be included, allowing a further finetuning of the flare rates and a reduction in the uncertainties in flare probability compared to the real-time McIntosh classification for the current day. Overall, the updated and homogenized flare rates and probabilities derived in this study should already help in making the operational forecasts by SWx services more accurate and reliable.

Acknowledgements

This work was supported by the Solar-Terrestrial Centre of Excellence (STCE, https://www.stce.be/). International Sunspot Numbers were obtained from SILSO, World Data Center – Sunspot Index and Long-term Solar Observations, Royal Observatory of Belgium, https://www.sidc.be/SILSO/home, 1976-present. The authors would like to thank Dr. Sabrina Bechet (SIDC/SILSO) for her contribution on the DigiSun project. Sunspot drawings were provided by the Kanzelhöhe Observatory, University of Graz, Austria. The USAF/NOAA sunspot data are courtesy of the Solar Cycle Science database (see Footnote 20). The "X-ray Flare" dataset was prepared by and made available through the NOAA National Centers for Environmental Information (NCEI), which since 2015 has also integrated the National Geophysical Data Center (NGDC). Data supplied for Figure 2 courtesy of SolarMonitor.org. SDO/AIA and SDO/HMI imagery used in this study courtesy of NASA/SDO and the AIA and HMI science teams. SDO is the first mission for NASA's Living With a Star (LWS) Program. SOHO/MDI and SOHO/EIT imagery used in this study courtesy of SOHO/MDI and SOHO/EIT consortia. SOHO is a project of international cooperation between ESA and NASA. The editor thanks Robert Steenburgh and an anonymous reviewer for their assistance in evaluating this paper.

Supplementary material

Supplementary materials of this article are available at https://www.swsc-journal.org/10.1051/swsc/2025007/olm.

This article contains four files with supplementary data.

The first file "Supplementary Data A_GOES flares_Old and New.xlsx" contains all 77775 flare events with the old and upscaled (new) flare intensities, as well as comments in the header cells providing additional clarifications. The last column "Not included" (also colour-coded in the first column) provides indications on how to get from the original batch of 77775 flares to the 37831 flares that would eventually be linked to the file with the McIntosh classifications. This basically means to ignore (1) flares with no intensity mentioned or "C0" in column "CMX old", (2) flares with no active region mentioned as the source, or after verification, no active region could be assigned ("Unk" in column "NOAA"), and (3) all A- and B-class flares in column "Class new only". These 3 subgroups have been labeled with respectively "1", "2" and "3" in the column "Not included".

The second file "Supplementary Data B_McIntosh classifications.xlsx" contains the McIntosh classifications for each of the 4720 "observing" days. This list contains 22232 genuine (i.e. non-zero) and 5088 "zero" (i.e. spotless days or the group in the NOAA listing had no corresponding group on the Kanzelhöhe drawing) McIntosh classifications.

The supplementary file "Suppl Mat_Results A_McI counts_upscaled(GOESNew)flarerates" tabulates for each McIntosh class the counts, the total number of flares associated with it (C, M, and X), the flare rate over 24 hours and the error following the methodology outlined in BL12. The next 3 columns represent the flare rate over 24 hours for C+ flares (C1 or higher flare, so summing for C- and M- and X-class flares), for M+ flares (M1 or higher flare, so summing for M- and X-class flares), and for X+ flares (the same as for X flares). The last columns are the error (BL12) and the McIntosh class again, which were added to guide the eye.

The fourth and final supplementary file "Suppl Mat_Results B_Flare probs_confidence intervals" tabulates for each McIntosh class the counts, the accumulated number of C-, M- and X-class flares ($\geq$ C1, $\geq$ M1, $\geq$ X1), and then for each of these 3 flare categories the Poisson flare probability and the corresponding confidence intervals (low, high). These probabilities are used by SWx forecast centers such as the SIDC.

References

Angryk RA, Martens PC, Aydin B, Kempton D, Mahajan SS, et al. 2020. Multivariate time series dataset for space weather data analytics. *Sci Data* **7**: 227. https://doi.org/10.1038/s41597-020-0548-x.

Aschwanden MJ. 1994. Irradiance observations of the 1–8 Å solar soft X-ray flux from GOES. *Sol Phys*, **152 (1)**: 53–59. https://doi.org/10.1007/BF01473183.

Barnes G, Leka KD, Schrijver CJ, Colak T, Qahwaji R,et al. 2016. A comparison of flare forecasting methods. I. Results from the "All-Clear" workshop. *Astrophys J* **829 (2)**: 89. https://doi.org/10.3847/0004-637X/829/2/89.

Bloomfield DS, Higgins PA, McAteer RTJ, Gallagher PT. 2012. Toward reliable benchmarking of solar flare forecasting methods. *Astrophys J Lett* **747 (2)**: L41. https://doi.org/10.1088/2041-8205/747/2/L41.

Boischot A. 1958. Étude du rayonnement radioélectrique solaire sur 169 MHz à l'aide d'un grand interféromètre à réseau. *Ann Astrophys* **21**: 273. https://ui.adsabs.harvard.edu/abs/1958AnAp...21..273B/abstract.

Bornmann PL. 1990. Limits to derived flare properties using estimates for the background fluxes: examples from GOES. *Astrophys J* **356**, 733–742. https://doi.org/10.1086/168880.

Bornmann PL, Shaw D. 1994. Flare rates and the Mcintosh active region classifications. *Sol Phys* **150** (**1–2**): 127–146. https://doi.org/10.1007/BF00712882.

Bornmann PL, Kalmbach D, Kulhanek D. 1994. McIntosh active region class similarities and suggestions for mergers. *Sol Phys* **150** (**1–2**): 147–164. https://doi.org/10.1007/BF00712883.

Bouwer SD. 1983. Intermediate-term epochs in solar soft X- ray emission. *J Geophys Res* **88 (A10)**: 7823–7830. https://doi.org/10.1029/JA088iA10p07823.

Canfield RC, Hudson HS, McKenzie DE. 1999. Sigmoidal morphology and eruptive solar activity. *Geophys Res Lett*, **26 (6)**: 627–630. https://doi.org/10.1029/1999GL900105.

Carrasco VMS, Lefèvre L, Vaquero JM, Gallego MC. 2015. Equivalence relations between the Cortie and Zürich sunspot group morphological classifications. *Sol Phys* **290 (5)**: 1445–1455. https://doi.org/10.1007/s11207-015-0679-y.

Carrington RC. 1859. Description of a singular appearance seen in the Sun on September 1, 1859. *Mon Not R Astron Soc* **20 (1)**: 13–15. https://doi.org/10.1093/mnras/20.1.13.

Cerruti AP, Kintner PM, Jr, Gary DE, Mannucci AJ, Meyer RF, et al. 2008. Effect of intense December 2006 solar radio bursts on GPS receivers. *Space Weather* **6**, 10. https://doi.org/10.1029/2007SW000375.

Clette F, Svalgaard L, Vaquero JM, Cliver EW. 2014. Revisiting the sunspot number. A 400-year perspective on the solar cycle. *Space Sci Rev* **186** (**1–4**): 35–103. https://doi.org/10.1007/s11214-014-0074-2.

Cliver EW, Schrijver CJ, Shibata K, Usoskin IG. 2022. Extreme solar events. *Living Rev Sol Phys* **19 (1)**, 2. https://doi.org/10.1007/s41116-022-00033-8.

Colak T, Qahwaji R. 2009. Automated Solar Activity Prediction: A hybrid computer platform using machine learning and solar imaging for automated prediction of solar flares. *Space Weather* **7**: 6. https://doi.org/10.1029/2008SW000401.

Cortie AL. 1901. On the types of sun-spot disturbances. *Astrophys J* **13**, 260. https://ui.adsabs.harvard.edu/link_gateway/1901ApJ....13..260C/doi:10.1086/140816.

Delaboudinière J-P, Artzner GE, Brunaud J, Gabriel AH, Hochedez JF, et al. 1995. EIT: extreme-ultraviolet imaging telescope for the SOHO mission. *Sol Phys* **162** (**1–2**): 291–312. https://doi.org/10.1007/BF00733432.

Devos A, Verbeeck C, Robbrecht E. 2014. Verification of space weather forecasting at the Regional Warning Center in Belgium. *J Space Weather Space Clim* **4**: A29. https://doi.org/10.1051/swsc/2014025.

Gallagher PT, Moon Y-J, Wang H. 2002. Active-region monitoring and flare forecasting I. Data processing and first results. *Sol Phys* **209 (1)**: 171–183. https://doi.org/10.1023/A:1020950221179.

Garcia HA. 1994.Temperature and emission measure from goes soft X-ray measurements. *Sol Phys* **154 (2)**: 275–308. https://doi.org/10.1007/BF00681100.

Giersch O, Kennewell J, Lynch M. 2018. Reanalysis of solar observing optical network sunspot areas. *Sol Phys* **293 (10)**: 138. https://doi.org/10.1007/s11207-018-1358-6.

Hale GE, Ellerman F, Nicholson SB, Joy AH. 1919. The magnetic polarity of sun-spots. *Astrophys J* **49**: 153. 10.1086/142452.

Hey JS. 1946. Solar radiations in the 4–6 metre radio wave-length band. *Nature* **157** (**3976**): 47–48. https://doi.org/10.1038/157047b0.

Hudson HS, Simões PJA, Fletcher L, Hayes LA, Hannah IG. 2021. Hot X-ray onsets of solar flares. *Mon Not R Astron Soc* **501 (1)**: 1273–1281. https://doi.org/10.1093/mnras/staa3664.

Janssens J. 2021. Prediction of the amplitude of solar cycle 25 using polar faculae observations. *J Space Weather Space Clim* **11**: 3. https://doi.org/10.1051/swsc/2020081.

Johnson NL, Kotz S. 1969. *Discrete distributions*. Boston: Houghton Mifflin Company, OCLC, p. 50253.

Kahler SW, Kreplin RW. 1991. The NRL SOLRAD X-ray detectors: A summary of the observations and a comparison with the SMS/GOES detectors. *Sol Phys* **133**: 371–384. https://doi.org/10.1007/BF00149895.

Kauristie K, Andries J, Beck P, Berdermann J, Berghmans D, et al. 2021. Space weather services for civil aviation – challenges and solutions. *Remote Sens* **13** (**18**): 3685. https://doi.org/10.3390/rs13183685.

Kiepenheuer KO. 1953. Solar activity. In: *The Sun, Chapter 6*, Kuiper GP (Ed.), The University of Chicago Press, Chicago, pp. 322–465. https://ui.adsabs.harvard.edu/abs/1953sun..book..322K/abstract.

Kildahl KJN. 1980. Solar activity predictions. In: *Solar-Terrestrial Predictions Proceedings*, Vol. **3**, Donnelly RF (Ed.), U.S. Department of Commerce, Boulder, pp. 166.

Kowalski AF. 2024. Stellar flares. *Living Rev Sol Phys*. **21 (1)**: 1. https://doi.org/10.1007/s41116-024-00039-4.

Kubo Y, Den M, Ishii M. 2017. Verification of operational solar flare forecast: case of Regional Warning Center Japan. *J Space Weather Space Clim* **7**: A20. https://doi.org/10.1051/swsc/2017018.

Künzel, H. 1960. Die Flare-Häufigkeit in Fleckengruppen unterschiedlicher Klasse und magnetischer Struktur. *Astron Nachr* **285 (5)**: 271. https://doi.org/10.1002/asna.19592850516.

Kusano, K, Iju T, Bamba Y, Inoue S. 2020. A physics-based method that can predict imminent large solar flares. *Science* **369 (6503)**: 587–591. https://doi.org/10.1126/science.aaz2511.

Lee, K, Moon Y-J, Lee J-Y, Lee K-S, Na H. 2012. Solar flare occurrence rate and probability in terms of the sunspot classification supplemented with sunspot area and its changes, *Sol Phys* **281 (2)**: 639–650. https://doi.org/10.1007/s11207-012-0091-9.

Lee, S, Lee J, Hong S. 2013. *ASSA GUI User Manual v.1.07*. Korean Space Weather Center. https://spaceweather.kasa.go.kr/images/assa/ASSA_GUI_MANUAL_112.pdf (last updated 14 September 2015; Version 1.12).

Leka, KD, Park S-H, Kusano K, Andries J, Barnes G, et al. 2019a. A comparison of flare forecasting methods. II. Benchmarks, metrics, and performance results for operational solar flare forecasting systems. *Astrophys J Suppl Ser* **243 (2)**: 36. https://doi.org/10.3847/1538-4365/ab2e12.

Leka, KD, Park S-H, Kusano K, Andries J, Barnes G, et al. 2019b. A comparison of flare forecasting methods. III. Systematic behaviors of operational solar flare forecasting systems. *Astrophys J* **881 (2)**: 101. https://doi.org/10.3847/1538-4357/ab2e11.

Lemen, JR, Title AM, Akin DJ, Boerner PF, Chou C, et al. 2012. The Atmospheric Imaging Assembly (AIA) on the Solar Dynamics Observatory (SDO). *Sol Phys* **275 (1–2)**: 17–40. https://doi.org/10.1007/s11207-011-9776-8.

Marqué, C, Klein K-L, Monstein C, Opgenoorth H, Pulkkinen A, et al. 2018. Solar radio emission as a disturbance of aeronautical radionavigation. *J Space Weather Space Clim* **8**: A42. https://doi.org/10.1051/swsc/2018029.

McCloskey, AE, Gallagher PT, Bloomfield DS. 2016. Flaring rates and the evolution of sunspot group McIntosh classifications. *Sol Phys* **291 (6)**: 1711–1738. https://doi.org/10.1007/s11207-016-0933-y.

McCloskey, AE, Gallagher PT, Bloomfield DS. 2018. Flare forecasting using the evolution of McIntosh sunspot classifications. *J Space Weather Space Clim* **8**: A34. https://doi.org/10.1051/swsc/2018022.

McIntosh, PS. 1990. The classification of sunspot groups. *Sol Phys* **125 (2)**: 251–267. https://doi.org/10.1007/BF00158405.

Meeus, J. 1958. Une formule d'adoucissement pour l'activité solaire. *Ciel et Terre* **74**: 445. http://adsabs.harvard.edu/abs/1958C%26T....74..445M.

Murray, SA, Bingham S, Sharpe M, Jackson DR. 2017. Flare forecasting at the Met Office Space Weather Operations Centre, *Space Weather* **15 (4)**: 577–588. https://doi.org/10.1002/2016SW001579.

Park, SH, Leka KD, Kusano K, Andries J, Barnes G, et al. 2020. A comparison of flare forecasting methods. IV. Evaluating consecutive-day forecasting patterns. *Astrophys J* **890**: 124. https://doi.org/10.3847/1538-4357/ab65f0.

Poppe BB. 2000. New scales help public, technicians understand space weather. *Eos, Trans Am Geophys Union* **81 (29)**: 322–328. https://doi.org/10.1029/00EO00247.

Poppe, BB, Jorden KP. 2006. *Sentinels of the Sun: forecasting space weather*. Johnson Books, Boulder. ISBN: 1-55566-379-6.

Qahwaji, R, Colak T. 2007. Automatic short-term solar flare prediction using machine learning and sunspot associations. *Sol Phys* **241 (1)**: 195–211. https://doi.org/10.1007/s11207-006-0272-5.

Ryan, DF, RO Milligan, Gallagher PT, Dennis BR, Tolbert AK, et al. 2012. The thermal properties of solar flares over three solar cycles using GOES X-ray observations. *Astrophys J Suppl* **202 (2)**: 11. https://doi.org/10.1088/0067-0049/202/2/11.

Sammis, I, Tang F, Zirin H. 2000. The dependence of large flare occurrence on the magnetic structure of sunspots. *Astrophys J* **540 (1)**: 583–587. https://doi.org/10.1086/309303.

Scherrer, PH, Bogart RS, Bush RI, Hoeksema JT, Kosovichev AG, et al. 1995. The solar oscillations investigation – Michelson doppler imager. *Sol Phys* **162 (1–2)**: 129–188. https://doi.org/10.1007/BF00733429.

Schou, J, Scherrer PH, Bush RI, Wachter R, Couvidat S, et al. 2012. Design and ground calibration of the helioseismic and magnetic imager (HMI) instrument on the solar dynamics observatory (SDO). *Sol Phys* **275 (1–2)**: 229–259. https://doi.org/10.1007/s11207-011-9842-2.

Stuart, A, Ord JK. 1994. *Kendall's Advanced Theory of Statistics* (6th Ed.). Hodder Education Publishers, United Kingdom. ISBN-10: 0340614307 / ISBN-13: 978-0340614303.

Toriumi, S, Wang H. 2019. Flare-productive active regions. *Living Rev Sol Phys* **16 (1)**: 3. https://doi.org/10.1007/s41116-019-0019-7.

Waldmeier, M. 1938. Chromosphärische Eruptionen. I. Mit 6 Abbildungen. *Z Astrophys* **16**: 276–290. https://ui.adsabs.harvard.edu/abs/1938ZA.....16..276W/abstract.

Waldmeier, M. 1947. Heliographische Karten der Photosphäre für das Jahr 1946. *Publikationen der Eidgen*össische Sternwarte Zürich **9**: 1.

Wheatland, MS, Litvinenko YE. 2002. Understanding solar flare waiting-time distributions. *Sol Phys* **211**: 255–274. https://doi.org/10.1023/A:1022430308641.

Wheatland, MS. 2005. A statistical solar flare forecast method. *Space Weather* **3**: 7. https://doi.org/10.1029/2004SW000131.

White, SM, Thomas RJ, Schwartz RA. 2005. Updated expressions for determining temperatures and emission measures from GOES Soft X-ray measurements. *Sol Phys* **227 (2)**: 231–248. https://doi.org/10.1007/s11207-005-2445-z.

Cite this article as: Janssens J, Delouille V, Clette F & Andries J. 2025. Solar flare rates and probabilities based on the McIntosh classification: Impacts of GOES/XRS rescaling and revisited sunspot classifications. *J. Space Weather Space Clim*. **15**, 14. https://doi.org/10.1051/swsc/2025007.

Appendix: Confidence interval for Poisson counts data: Application to flare rate and flare probabilities

A.1 Flares follow a Poisson distribution

Let Y denote the GOES flux (in W/m^2). There is a C-class flare when $a_C = 10^{-6} \leq Y \leq b_C = 10^{-5}$, an M-class flare when $a_M = 10^{-5} \leq Y \leq b_M = 10^{-4}$ and an X-class flare when $Y \geq a_X = 10^{-4}$.

We are interested in the exceedance probability, that is, the probability that during a given time interval, the Sun produces at least one flare of class C or higher (C+), at least one M-class flare or higher (M+), and at least one X-class flare (X+).

Flares are usually produced in active regions (AR). The greater the complexity of the AR, the more likely it will produce flares. Let Z_i be the number of flares of class C+ that are going to occur during this time interval in the i-th AR that is observed on the Sun, and let τ be the total number of ARs observed on the solar disc during this time interval ($i = 1, \ldots, \tau$). The total probability of having at least one C+ flare is:

$$P_{\text{tot,C+}} = 1 - P(\text{zero C+ flare}) = 1 - \prod_{i=1}^{\tau} P(Z_i = 0),$$

and similarly, we can compute $P_{\text{tot,M+}}$ and $P_{\text{tot,X+}}$. In practice, we consider one day (24 hours) as a unit of time interval.

The complexity of an AR may be characterized by the McIntosh classification, which separates the AR into classes using properties such as unipolarity or bipolarity, presence of a penumbra, its size and symmetry, sunspot distribution between the two poles of the AR. For a given class of McIntosh, one may assume as a first approximation that the corresponding AR will produce flares with a constant mean rate, independently of the time since the last observed flare was observed. In other words, we assume that the number of flares of a given class follows a Poisson distribution (Gallagher et al., 2002).

Let λ be the mean flare rate associated with a given McIntosh class, and let X be the number of flares that are going to occur in the forthcoming 24 hours in an AR of this given McIntosh class. Since we assume $X \sim \text{Po}(\lambda)$, we have:

$$P(X \geq 1) = 1 - P(X = 0) = 1 - \exp(-\lambda). \tag{A.1}$$

If we have an estimate and Confidence Interval (CI) on λ, by equation (A.1), we immediately obtain an estimation of the probability and Confidence Interval of having at least one flare. To get CI on λ, we need to compute the mean and variance of the estimator of λ.

A.2 Mean and variance of mean flare rate estimator

Suppose we have observed during N_t days an AR of a given McIntosh class, and out of these N_t days, the AR has flared n times. Let X be the number of times an AR produces a flare when observed on a particular day (24-hour period). We assume that X follows a Poisson law with rate λ. As estimate for λ, we use the empirical mean:

$$\hat{\lambda} = \hat{X} = \frac{1}{N_t}\sum_{i=1}^{N_t} X_i = \frac{n}{N_t}, \tag{A.2}$$

where X_i denotes the number of flares observed on day i. To obtain a CI for $\hat{\lambda}$, we need to know the distribution of $\hat{\lambda}$. We know that if $X \sim \text{Po}(\lambda)$, and we have N_t independent and identically distributed variables that are all $\text{Po}(\lambda)$, then the distribution of $\sum_{i=1}^{N_t} X_i \sim \text{Po}(N_t\lambda)$, with expectation $N_t\lambda$ and variance $N_t\lambda$. Thus, the expectation of $\hat{\lambda}$ is equal to $N_t\lambda/N_t = \lambda$ (i.e. this estimator is without bias), and its variance is equal to:

$$\text{Var}\left(\hat{\lambda}\right) = \text{Var}\left(\frac{1}{N_t}\sum_{i=1}^{N_t} X_i\right) = \frac{1}{N_t^2}\text{Var}\left(\sum_{i=1}^{N_t} X_i\right) = \frac{1}{N_t^2} N_t\lambda = \frac{\lambda}{N_t}. \tag{A.3}$$

Since the empirical estimate of λ is n/N_t, by plug-in into equation (A.3), we have the following estimate for the variance and standard deviation of $\hat{\lambda}$:

$$\hat{\text{Var}}\left(\hat{\lambda}\right) = \frac{n}{N_t^2}, \qquad \hat{\sigma}\left(\hat{\lambda}\right) = \frac{\sqrt{n}}{N_t}. \tag{A.4}$$

A.3 Confidence interval

A.3.1 Gaussian approximation

Here λ is not so large, but n can be large. For $n \geq 20$, we can use the Gaussian approximation for $\hat{X}$:

$$\hat{X} \sim \aleph\left(n/N_t, \sqrt{n}/N_t\right),$$

with thus a 95% CI on λ that takes the form of:

$$[n/N_t - 1.96\sqrt{n}/N_t,\ n/N_t + 1.96\sqrt{n}/N_t]. \tag{A.5}$$

The corresponding CI on the probability of having at least one flare is obtained by computing equation (A.1) for the lower and upper value of the CI in equation (A.5).

A.3.2 Exact computation using Chi-square

When a small number of events ($n < 20$) are observed for a particular McIntosh class, one should use the relationship between the chi-square and Poisson distributions (Johnson & Kotz, 1969; Stuart & Ord, 1994) rather than the approximation with the normal distribution.[24]

Let n be the number of flares observed, and $\chi(df, \alpha)$ be the X^2 distribution with degree of freedom df and significance level α. We are first looking for 95% CI interval for n, which is obtained as follows:

$$\text{CI}(n) = \left[0.5 * q\left(\chi^2_{2n,\frac{\alpha}{2}}\right),\ 0.5 * q\left(\chi^2_{2(n+1),1-\frac{\alpha}{2}}\right)\right], \tag{A.6}$$

where $q()$ denotes the quantile function, that is, the inverse of the probability distribution function. By dividing equation (A.6) by N_t we obtain a CI on λ, and again by using equation (A.1) we obtain the corresponding CI on the probability of having at least one flare.

[24] See also the explanation in https://onbiostatistics.blogspot.com/2014/03/computing-confidence-interval-for.html.